

**THE MINERALOGICAL CONSEQUENCES AND BEHAVIOR
OF DESCENDING ACID-SULFATE WATERS: AN EXAMPLE
FROM THE KARAHA – TELAGA BODAS GEOTHERMAL SYSTEM, INDONESIA**

JOSEPH N. MOORE[§]

Energy & Geoscience Institute, 423 Wakara Way, Suite 300, Salt Lake City, Utah 84108, U.S.A.

BRUCE W. CHRISTENSON

Rafter Isotope Laboratory, Institute of Geological and Nuclear Sciences, Lower Hutt, New Zealand

RICHARD G. ALLIS

Utah Geological Survey, Salt Lake City, Utah 84114, U.S.A.

PATRICK R.L. BROWNE

Geology Department, University of Auckland, Private Bag 92019, Auckland, New Zealand

SUSAN J. LUTZ

Energy & Geoscience Institute, 423 Wakara Way, Suite 300, Salt Lake City, Utah 84108, U.S.A.

ABSTRACT

Acidic steam condensates in volcanic systems or shallow, oxygenated geothermal environments are typically enriched in SO₄ and poor in Cl. These fluids produce distinctive alteration-induced assemblages as they descend. At Karaha – Telaga Bodas, located on the flank of Galunggung Volcano, Indonesia, neutralization of descending acid waters has resulted in the successive appearance of 1) advanced argillic alteration characterized by alunite, clay minerals and pyrite, 2) anhydrite, pyrite and interlayered sheet silicates, and 3) carbonates. Minor tourmaline, fluorite and native sulfur also are present locally, reflecting interactions with discharging magmatic gases. Water–rock interactions were modeled at temperatures up to 250°C using the composition of acidic lake water from Telaga Bodas and that of a typical andesite as reactants. The simulations predict mineral distributions consistent with the observed assemblages and a decrease in the freezing-point depression of the fluid with increasing temperature. Fluids trapped in anhydrite, calcite and fluorite display a similar decrease in their freezing-point depressions, from 2.8° to 1.5°C, as homogenization temperatures increase from 160° to 205°C. The simulations indicate that the progressive change in fluid composition is due mainly to the incorporation of SO₄ into the newly formed hydrothermal minerals. The salinities of fluid inclusions containing Cl-deficient steam condensates are better expressed in terms of H₂SO₄ equivalents than the commonly used NaCl equivalents. At solute concentrations >1.5 molal, freezing-point depressions represented as NaCl equivalents overestimate the salinity of Cl-poor waters. At lower concentrations, differences between apparent salinities calculated as NaCl and H₂SO₄ equivalents are negligible.

Keywords: acid-sulfate waters, vapor-dominated, geothermal systems, fluid inclusions, Karaha – Telaga Bodas, Indonesia.

SOMMAIRE

Les produits de condensation de vapeur acide des systèmes volcaniques ou des milieux géothermiques oxygénés à faible profondeur sont typiquement enrichis en SO₄ et appauvris en Cl. Ces fluides produisent des assemblages distinctifs de minéraux d'altération à mesure qu'ils atteignent les parties profondes du système. A Karaha – Telaga Bodas, situé sur le flanc du volcan Galunggung, en Indonésie, la neutralisation des eaux descendantes acides a mené à la formation successive 1) d'une altération argillique avancée, et une association d'alunite, d'argiles et de pyrite, 2) d'anhydrite, de pyrite et de phyllosilicates interstratifiés, et 3) de carbonates. Des quantités moindres de tourmaline, de fluorite et de soufre sont aussi présentes, témoins d'interactions

[§] E-mail address: jmoore@egi.utah.edu

avec des décharges de gaz magmatiques. Les interactions d'eau et de roche ont été simulées à des températures jusqu'à 250°C en utilisant la composition de l'eau de lac à Telaga Bodas et une andésite typique comme réactifs. Les simulations prédisent une distribution de minéraux conforme aux assemblages observés et une diminution du point de congélation de la phase fluide avec une augmentation de la température. La phase fluide piégée dans l'anhydrite, la calcite et la fluorite font preuve d'une diminution semblable du point de congélation, de 2.8° à 1.5°C, à mesure que la température d'homogénéisation augmente, de 160° à 205°C. D'après ces simulations, le changement progressif dans la composition de la phase fluide serait surtout dû à l'incorporation de SO₄ dans les minéraux hydrothermaux néoformés. On exprimerait mieux la salinité des inclusions fluides contenant des condensés de vapeur à faible teneur en Cl en termes d'équivalents de H₂SO₄ plutôt que d'équivalents de NaCl, d'utilisation répandue. A une concentration du soluté dépassant 1.5 en molalité, l'abaissement du point de congélation où l'équivalence est exprimée en termes de NaCl mène à une surestimation de la salinité des eaux à faible teneur en Cl. A plus faibles teneurs, les différences entre la salinité calculée en supposant une équivalence de NaCl et celle en supposant une équivalence de H₂SO₄ sont négligeables.

(Traduit par la Rédaction)

Mots-clés: eaux sulfatées acides, domination de vapeur, système géothermique, inclusions fluides, Karaha – Telaga Bodas, Indonésie.

INTRODUCTION

Acid-sulfate steam condensates are a ubiquitous feature of geothermal and volcanic systems. Condensates produced by the boiling of hydrothermal fluids typically contain SO₄ as their dominant anion, derived from the oxidation of ascending H₂S, and H as the main cation (*e.g.*, Ellis & Mahon 1977). In contrast to the deep reservoir fluids, Cl concentrations in the condensates are generally negligible. Condensates and crater lakes associated with actively degassing magmas, on the other hand, contain SO₄ derived from the disproportionation of magmatic SO₂, as well as through oxidation of H₂S and intermediate oxyanions of S (Kusakabe *et al.* 2000, Christenson 2000). In addition, variable concentrations of Cl, F and B can be introduced through dissolution of magmatic gas species (HCl, HF and H₃BO₃, respectively) and by dissolution of the host rocks (Hedenquist 1995, Christenson *et al.* 2002).

Advanced argillic alteration is diagnostic of interactions between acid-sulfate waters and the enclosing wallrocks (Hemley *et al.* 1969, 1980). Characteristic minerals include kaolinite, dickite, pyrophyllite, natroalunite, alunite, diaspore, andalusite, pyrite and enargite (Reyes 1990, 1991). Alteration considered to be produced by the descent of acid-sulfate waters occurs as deep as 2500 m in active Philippine geothermal systems, although depths of 1600 to 1800 m appear to be more typical (Reyes 1991). These descending fluids may remobilize previously deposited ore minerals. For example, in the sediment-hosted micrometric gold deposits in Nevada, descending surficial acid-sulfate waters concentrated gold deposited by earlier hydrothermal fluids (Arehart *et al.* 1992, Ebert & Rye 1997).

However, similar assemblages form where high-temperature magmatic volatiles dissolve into the surrounding groundwaters at depth (Christenson & Wood 1993). In volcanic environments, the formation of acid-sulfate waters marginal to cooling magmas can lead to the formation of vuggy silica rock with high permeabilities and

porosities. This process may be a prerequisite for the formation of high-sulfidation ore deposits (Hayba *et al.* 1985, Stoffregen 1987, White & Hedenquist 1990, Hedenquist *et al.* 1994).

Despite the ubiquitous occurrence of advanced argillic alteration and acidic steam condensates in many volcanic-rock-hosted geothermal fields, and evidence of their presence in many epithermal deposits, the thermal and chemical evolution of these fluids as they descend has not yet been well characterized. In this paper, we first describe mineralogical and fluid-inclusion data from the active geothermal system at Karaha – Telaga Bodas, Indonesia, where advanced argillic alteration related to descending acid-sulfate water is locally well developed. The results of numerical simulations conducted to characterize the interactions occurring between the steam condensate and the wall rocks are then presented. Finally, we combine the results of the simulations with the petrological data to develop the most appropriate methodologies for interpreting fluid-inclusion freezing temperatures in this environment.

ANALYTICAL METHODS

Heating and freezing measurements were performed on fluid inclusions trapped in quartz, anhydrite, calcite and fluorite. Inclusions in doubly polished plates of individual crystals hand-picked from the drill cores were studied. Measurements were made on a Linkam THSMG 600 heating and freezing stage calibrated with synthetic fluid inclusions. The precision of the measurements is estimated to be ±0.1°C at 0.0°C and ±3°C at 374°C. Only measurements made on liquid-rich inclusions are reported. The salinity of two-phase inclusions with ice-melting temperatures greater than -21.2°C was calculated using the equation presented by Bodnar (1993). A few inclusions in quartz yielded ice-melting temperatures less than -21.2°C. These inclusions displayed initial ice-melting temperatures near -50°C, suggesting the presence of Ca, Mg or Fe in addition to Na.

The salinity of these inclusions was approximated from relationships in the system $H_2O-NaCl-CaCl_2$ (Yanatieva 1946). The composition of the halite-bearing inclusions was calculated from halite-dissolution temperatures using the equation of Sterner *et al.* (1988).

Samples for electron-microprobe analyses were prepared as polished grains in epoxy mounts. The analyses were performed at the University of Utah on a Cameca SX-50 electron-microprobe micro-analyzer (EMPA) with four multicrystal spectrometers. Instrument conditions were: accelerating voltage 15 kV, beam current 20 nA and beam diameter 1 to 20 μm . A suite of natural minerals was used as standards. Concentrations were calculated from intensities using the phi method of Pouchou & Pichoir (1991).

Scanning electron microscope (SEM) images and semiquantitative analyses by energy-dispersion spectroscopy (EDS) have provided additional information on the textural relationships, mineral morphologies, and scale and mineral compositions. A small, freshly broken portion of each sample was mounted on a standard SEM mount and coated with C. The samples were examined on a Philips XL30 Environmental Scanning Electron Microscope (ESEM) at the Idaho National Engineering and Environmental Laboratory. This instrument is equipped with a Princeton Gamma Tech Prism system. An accelerating voltage of 20 kV and a beam diameter of 3 μm were utilized. A ZAF correction procedure was used to reduce the elemental compositions.

The composition of the lake water from Telaga Bodas was determined by standard chemical techniques. Levels of Ca, Mg, Na, K, SiO_2 , As, Fe and Sr were established by atomic absorption spectrophotometry. The concentration of SO_4 was determined by ion chromatography. The samples were analyzed for Cl by titration, and for B and NH_4 by colorimetric spectrophotometry.

THE KARAHA – TELAGA BODAS GEOTHERMAL SYSTEM

Geological and hydrological relationships

Karaha – Telaga Bodas is a partially vapor-dominated geothermal system located on the flank of Galunggung Volcano in western Java, Indonesia. Since 1822, the volcano has erupted five times. Kawah Galunggung, the main vent, is a horseshoe-shaped crater that formed when the flank of the volcanic edifice collapsed (Escher 1925). The resulting debris-avalanche flow produced extensive hummocky deposits southeast of the crater known as “The Thousand Hills of Tasikmalaya”. Charcoal from a pyroclastic flow considered to have been deposited shortly after flank collapse has yielded a ^{14}C age of 4200 ± 150 years BP (Bronto 1989).

Geothermal exploration has focused on the volcanic ridge that extends northward from Kawah Galunggung.

During the late 1990s, the Karaha Bodas Co. LLC drilled 29 exploration and production wells, with some reaching depths of nearly 3 km (Fig. 1). Thermal features associated with the discharge of steam and steam condensates occur at the southern and northern ends of the prospect, approximately 10 km apart. At the southern end, 5 km north of Kawah Galunggung, these thermal features include the fumaroles at Kawah Saat, an acidic lake (Telaga Bodas) and acid Cl- SO_4 springs. Elevated concentrations of F, Cl and SO_4 in the lake water (unpubl. data, Karaha Bodas Co. LLC) and nearby wells indicate that magmatic gases influence the lake’s composition. Kawah Karaha, a smaller fumarole field, is located at the northern end of the prospect. HCO_3 -rich waters discharge from springs at Kawah Karaha.

Allis *et al.* (2000) presented a conceptual model of the geothermal system based on measured downhole temperatures and pressures (Fig. 2). They showed that the geothermal system consists of a caprock characterized by steep thermal gradients and low permeabilities, an extensive vapor-dominated regime and a deeper liquid-dominated reservoir. North of Telaga Bodas, the low permeability of the caprock precludes significant downward percolation and flooding of the steam zone by condensates and meteoric waters. At Telaga Bodas, where the caprock is breached, acid-sulfate waters descend into the upper parts of the reservoir, but because of the high temperatures and low pressures, they boil off at relatively shallow depths.

Vapor-dominated conditions extend beneath the entire explored portion of the prospect to depths below sea level. The highest measured temperatures (353°C) and pressures are found in drill hole TLG 2-1, located closest to Telaga Bodas, where the steam zone is thickest (Fig. 2). Wells producing from the vapor-dominated regime discharge dry steam at vaporstatic pressures. Allis *et al.* (2000) suggested that a magmatic chimney cores the vapor-dominated zone beneath Telaga Bodas. Because the vapor-dominated zone is significantly underpressured relative to local hydrostatic conditions, low-permeability seals must envelop the steam-bearing rocks.

Deep wells drilled into the liquid-dominated resource in the northern half of the area discharge waters with total dissolved solid contents of 1 to 2 wt. % and $\delta^{18}O$ values of -5 to -1‰ (Powell *et al.* 2001). The $\delta^{18}O$ values were calculated from isotopic analyses of the separated steam and water corrected to the total discharge, assuming isotopic equilibrium at the conditions of separation. On the basis of the isotopic data, Powell *et al.* (2001) suggested that the deep waters are dominantly meteoric in origin and that the fluids in the southern part of the field contain an appreciable magmatic component, which is absent in the north. The liquid reservoir is underpressured by ~ 30 bars relative to a cold hydrostatic column beneath the adjacent valley floor. This pressure difference results in the flow of deep re-

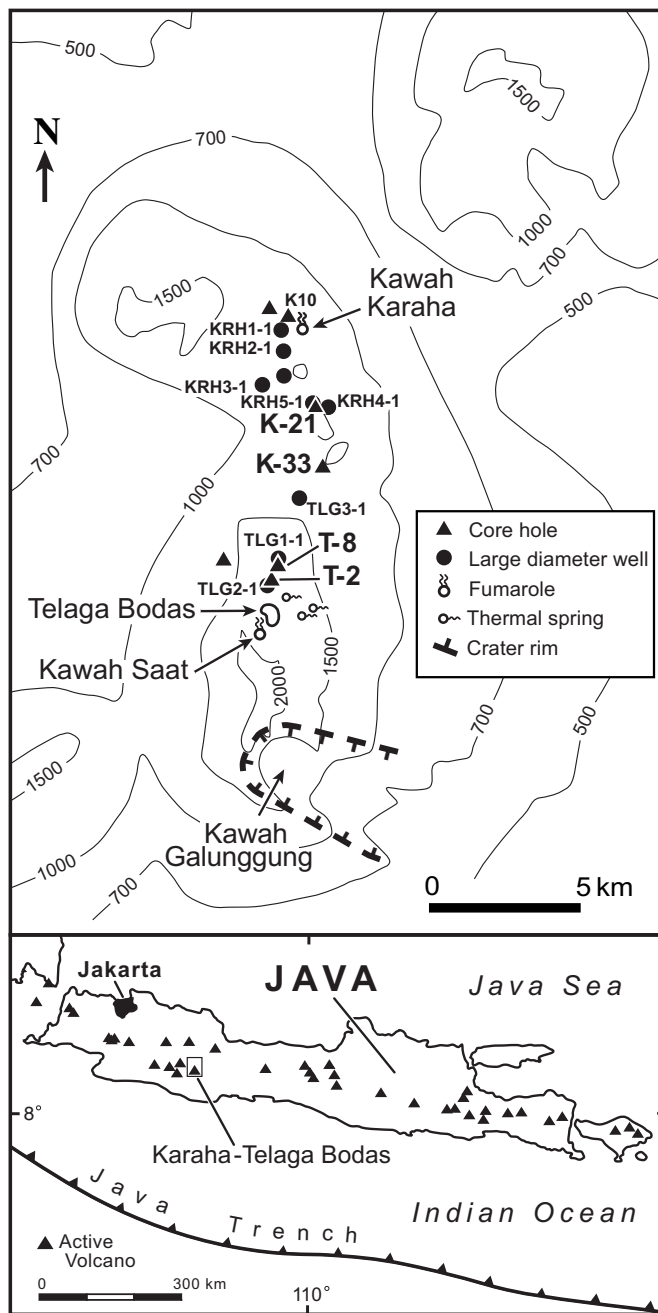


FIG. 1. Map illustrating the distribution of volcanic features, thermal manifestations and geothermal wells at Karaha – Telaga Bodas. Kawah Galunggung is the main vent of Galunggung Volcano. Telaga Bodas is an acid lake. Acid Cl-SO_4 springs discharge down-slope of Telaga Bodas. Only wells shown on the cross-section in Figure 2 are plotted. KRH- and TLG-series wells are deviated, rotary-drilled large-diameter wells. T and K series wells are vertical core holes. Contour lines show elevations in meters above sea level (m asl). Core holes in bold type are discussed in the text. Modified from Allis *et al.* (2000).

charging waters toward Telaga Bodas, which acts as a local pressure-sink.

The volcanic rocks that host the geothermal system at Karaha – Telaga Bodas consist mainly of pyroclastic and epiclastic deposits. Andesitic to basaltic lava flows are widely distributed at depth, but were less commonly encountered in the wells. Fine-grained sediments deposited in isolated basins are locally interbedded with the volcanic rocks. Organic matter in lake beds encountered in core holes T-8 and K-33 has yielded ^{14}C ages ranging from $41,500 \pm 1200$ to $5,910 \pm 76$ years BP (Fig. 2; Moore *et al.* 2002a). All of these deposits underlie volcanic rocks altered by high temperature ($>300^\circ\text{C}$) fluids. The youngest date was obtained on a deposit encountered at a depth of 988.5 m in core hole T-8. These dates demonstrate that intrusive activity, and significant hydrothermal alteration and volcano building, occurred during the recent past.

Hypabyssal intrusive rocks underlie much of the Karaha – Telaga Bodas area. Coarse-grained granodiorite was encountered at depths of ~ 3 km in the northern wells (Fig. 2). Intrusion of the granodiorite was accompanied by contact metamorphism of the surrounding volcanic rocks and the deposition of assemblages of high-temperature minerals. Intrusive rocks were not found in the southernmost wells. However, the occur-

rence of similar assemblages at relatively shallow depths in drill hole TLG 2-1, and modeling of a pronounced circular gravity anomaly near Telaga Bodas (Tripp *et al.* 2002), suggest that intrusive rocks lie closest to the surface in the southern part of the geothermal area.

Mineralogical relationships

Moore *et al.* (2000a, 2002a) described the hydrothermal alteration in the geothermal system. They recognized three distinct stages in the system's evolution. The oldest assemblages record the development of an extensive, high-temperature liquid-dominated system. At the shallowest depths, the wallrocks are altered to mixtures of clay minerals, chlorite, pyrite and quartz. Pyroclastic and epiclastic deposits are more highly altered than the lava flows. Veins in the upper parts of the geothermal system are dominated by calcite and zoned with chlorite + pyrite + quartz + calcite on the vein margins and later calcite + hematite within the vein interiors. Marginal calcite veins are commonly associated with CO_2 -rich steam-heated waters that envelop the high-temperature cores of geothermal systems (*e.g.*, Mahon *et al.* 1980, Hedenquist 1990). Propylitic assemblages consisting of chlorite, epidote, apatite, amphiboles, plagioclase, pyrite, quartz, prehnite and garnet occur in

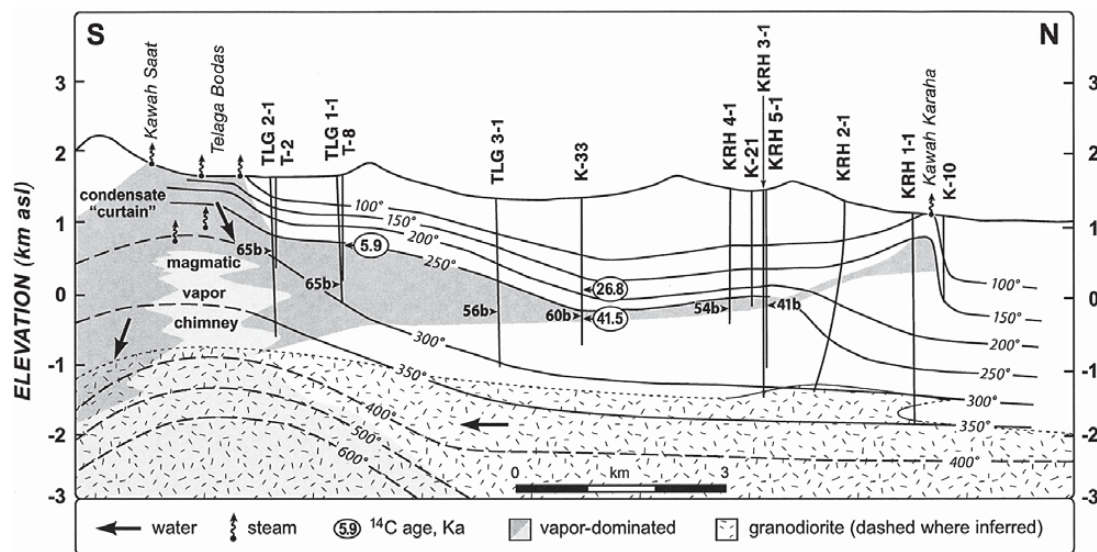


FIG. 2. Generalized north-south cross-section of the Karaha – Telaga Bodas geothermal field depicting the subsurface conditions and major hydrological features. Temperatures in $^\circ\text{C}$ are shown as solid lines where measured, and dashed where inferred. Regions in shades of gray are vapor-dominated. The magmatic vapor chimney is shown in light gray; surrounding portions of the vapor-dominated zone are dark gray. Measured spot pressures within the vapor-dominated region are given in bars (b). Wells KRH 1-1, KRH 2-1 and KRH 3-1 penetrated the top of the granodiorite. High-temperature alteration assemblages in wells TLG 1-1, TLG 2-1 and TLG 3-1, which indicate proximity to the intrusion, and the modeling of gravity data (Tripp *et al.* 2002), provide constraints on the depth and geometry of the granodiorite in the southern part of the field. Modified from Allis *et al.* (2000).

the wallrocks and veins at depths as shallow as 850 m. Epidote is diagnostic of neutral-pH fluids with temperatures $>250^{\circ}\text{C}$; amphiboles typically do not become stable until temperatures reach $\sim 300^{\circ}\text{C}$ (Henley & Ellis 1983). Potassic assemblages first appear at depths as shallow as ~ 1150 m in core hole T-8. Veins and wallrock assemblages in this zone contain biotite, epi-

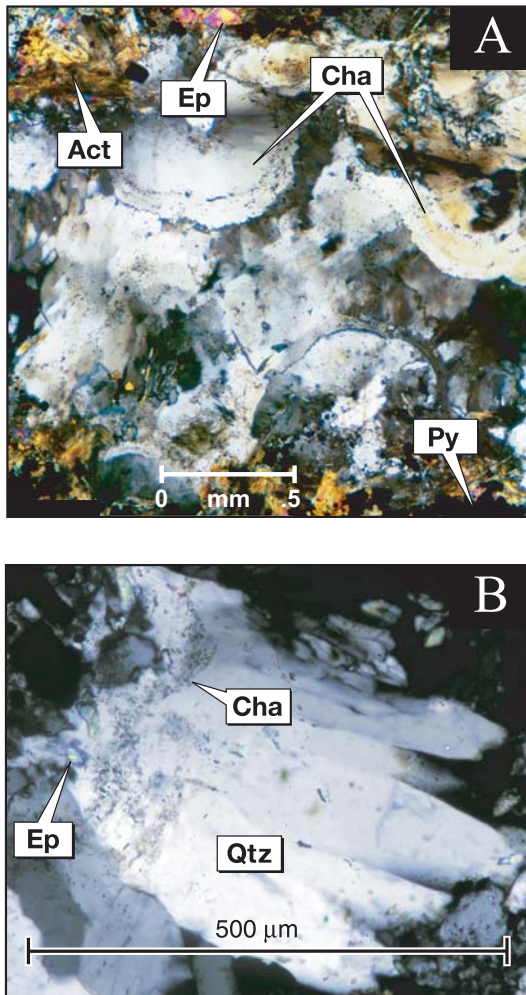


FIG. 3. Quartz veins displaying botryoidal textures indicating deposition as chalcedony or possibly amorphous silica. A) Vein cutting wallrocks containing the high-temperature alteration assemblage epidote + actinolite + pyrite. From a depth of 1139 m in core hole T-8. Crossed nicols. B) Quartz overgrowths on chalcedony. Botryoidal textures are preserved in the cores of the crystals. A grain of epidote is encapsulated in the chalcedony. From a depth of 1203 m in core hole T-8. Crossed nicols. Abbreviations: act: actinolite, cha: chalcedony, epi: epidote, qtz: quartz, py: pyrite.

dote, amphiboles and sporadic occurrences of clinopyroxene, garnet, talc, magnetite, cubanite and galena. This alteration assemblage records temperatures above 325°C . At still higher temperatures, within ~ 300 m of the granodiorite, coarse-grained blue-green tourmaline is found.

The second stage in the evolution of the geothermal system marks the transition from liquid- to vapor-dominated conditions. Amorphous silica, microcrystalline quartz (“chalcedony”) and euhedral crystals of quartz that commonly display complex twinning, curved *c* axes and epitactic growth dominate the mineral assemblages deposited during this stage. At depths of <800 m in core hole K-21, botryoidal masses of interlayered amorphous silica and “chalcedony” are the characteristic phases. Locally, they are associated with fine-grained quartz. At greater depths in core hole K-21 and in other wells, no direct evidence for the deposition of amorphous silica has been observed. However, botryoidal textures are preserved in quartz veins (Fig. 3A) and the core of euhedral quartz crystals throughout the field (Fig. 3B). Botryoidal textures could have formed during the deposition of either “chalcedony” or amorphous silica that was subsequently converted to quartz by the high geothermal temperatures. Irrespective of its origin, the term “chalcedony” is used to characterize silica phases displaying botryoidal textures; although not an IMA-approved name, it is used hereafter without quotation marks.

Chalcedony and later quartz are widely distributed. They have been found throughout core holes T-2, T-8, K-33 and K-21, which reach depths up to 2018 m. Their distribution in the deeper parts of the system, however, is not well established because vein textures are poorly preserved in the very fine-grained cuttings sampled from the large-diameter rotary drilled wells. Both the chalcedony and quartz encapsulate earlier high-temperature alteration-induced phases, including epidote and actinolite in core holes T-2 and T-8 (Fig. 3), and prehnite after epidote in K-33. At shallow depths, the chalcedony is locally intergrown with chlorite, whereas in the deeper parts of the system, it is not uncommon to find quartz intergrown with traces of epidote, chlorite, “sericite”, calcite, prehnite, wairakite and anhydrite. Coprecipitation of calcite and quartz is indicative of boiling. With the exception of wairakite and anhydrite, which are characteristic of stage-3 assemblages, the minerals that coprecipitated with quartz were among the last minerals deposited in the wallrocks and veins prior to quartz deposition. No mineralogical evidence of a hiatus or of significant cooling has been observed in quartz crystals containing a core of chalcedony, and the mineral assemblages associated with quartz suggest that temperatures remained elevated throughout deposition of the silica phases. These textural observations imply that the deposition of chalcedony and quartz represents a single continuous high-temperature event.

Fluid inclusions suitable for study were not observed in chalcedony, and it is likely that those present represent processes occurring after its formation (Fournier 1985, Sanders & Black 1988). The quartz crystals, however, contain abundant two-phase liquid- and vapor-rich inclusions, and in many samples, vapor-rich inclusions dominate. Rarely, the liquid-rich inclusions contain daughter crystals. Fluorite is the most common; halite or sylvite, which are characteristic of magmatic environments, have not been observed. Homogenization temperatures and salinities of the liquid-rich inclusions range from 235° to ~350°C and 0 to ~24 wt.% NaCl–CaCl₂ equivalent (Moore *et al.* 2000a). Inclusions with salinities exceeding 3 wt.% NaCl equivalent are common in core hole T–8. In contrast, high-salinity inclusions are only occasionally observed in core hole T–2 and appear to be absent in core holes K–33 and K–21, drilled in the central and northern parts of the field.

Moore *et al.* (2000a) concluded that the homogenization temperatures of the quartz-hosted inclusions closely approximate the conditions prevailing at the time of chalcedony deposition. On the other hand, they suggested that the broad range of salinities found in core hole T–8 more likely reflected the progressive concentration of early, relatively dilute fluids as they boiled toward dryness. Low-salinity inclusion fluids were interpreted as representing various proportions of meteoric waters and steam condensates. Although the waters that deposited chalcedony were probably also dominantly meteoric in origin, relationships between N₂:Ar and Ar:He ratios of quartz-hosted fluid inclusions document the presence of a magmatic contribution (Moore *et al.* 2002b).

Quartz is the silica phase that commonly forms at temperatures above 225°C (Fournier 1985). The deposition of chalcedony at the higher temperatures recorded by the fluid inclusions requires oversaturation of silica with respect to quartz (Fournier 1973), a condition not normally encountered in the deeper portions of high-temperature geothermal fields. Silica oversaturation may result from cooling or boiling. The mineral parageneses, the abundance of vapor-rich fluid inclusions, and the high salinity of the inclusion fluids indicate that the most likely cause of silica oversaturation was the massive flashing of water to steam during decompression. Furthermore, the widespread occurrence of chalcedony demonstrates that decompression was a field-wide event.

The lake beds deposited at 5910 ± 76 years BP provide constraints on the age of the early liquid-dominated system (stage 1) and its decompression (refer to Fig. 2; Moore *et al.* 2002a). These deposits underlie rocks containing chalcedony and earlier actinolite and epidote. However, no extraordinary volcanic eruptions are known to have occurred during the last 5900 years, and the absence of multiple episodes of chalcedony deposition implies that past eruptions were of insufficient magnitude to cause widespread decompression of the

early liquids. Thus it is more likely that decompression was associated with the flank collapse that resulted in the formation of the volcano's crater, Kawah Galunggung, at 4200 years BP (Bronto 1989).

As the pressures within the geothermal system declined, anhydrite, pyrite, calcite and wairakite were deposited throughout the field. These minerals overprint quartz and chalcedony and characterize the third stage in the evolution of the system. Anhydrite and calcite, which generally form monomineralic or mineralogically simple veins, have retrograde solubilities. Their parageneses indicate that deposition occurred in response to the heating of descending waters.

Although the late hydrothermal history of the rocks throughout the field is generally similar, mineral assemblages in core hole T–2 record evidence of interactions with both shallow acidic waters and magmatic volatiles that are not found elsewhere. These effects appear to be related to the proximity of the core hole to Telaga Bodas, which is considered to be fed by a magmatic vapor chimney (Allis *et al.* 2000). The most significant mineralogical differences are the presence of advanced argillic alteration, fluorite, native sulfur and tourmaline. This paragenetically late tourmaline is distinctive and unrelated to earlier-formed, high-temperature tourmaline found near the intrusive contact.

The occurrence of the advanced argillic alteration documents interactions with aggressive acid-sulfate condensates. This alteration is common in the upper 350 m of the core hole, and between 200 and 350 m, it is intense and pervasive. For comparison, the distribution of mineral assemblages to a depth of 900 m, where measured temperatures reach 250°C, is shown in Figure 4. At greater depths, only propylitic and potassic assemblages are present. Core hole T–2 was drilled to a depth of 1383 m, reaching an elevation of 288 m above sea-level (m asl). It has a measured bottom-hole temperature of 321°C (Fig. 2).

We have assigned the advanced argillic alteration to stage 3, despite the absence of clear cross-cutting relationships with stage-1 and stage-2 assemblages. This assumption is based on: 1) an association with stage-3 anhydrite and pyrite, 2) the occurrence of highly acidic waters in Telaga Bodas, and 3) the results of numerical simulations presented below that predict relationships consistent with the observed mineral distributions and parageneses.

Advanced argillic alteration is only weakly developed in the upper 200 m of core hole T–2. Minor kaolinite and smectite, and traces of alunite, jarosite and poorly crystalline imogolite and allophane-type minerals have been identified. X-ray-diffraction analysis of the kaolinite-group minerals suggests that some halloysite and dickite may also be present in this interval. The alunite-group minerals occur primarily in thin veins. At greater depths, between 200 and 340 m, the alteration assemblage consists of quartz, increased concentrations of alunite, natroalunite, kaolinite, pyrite and sepiolite. Natroalunite persists sporadically to a depth

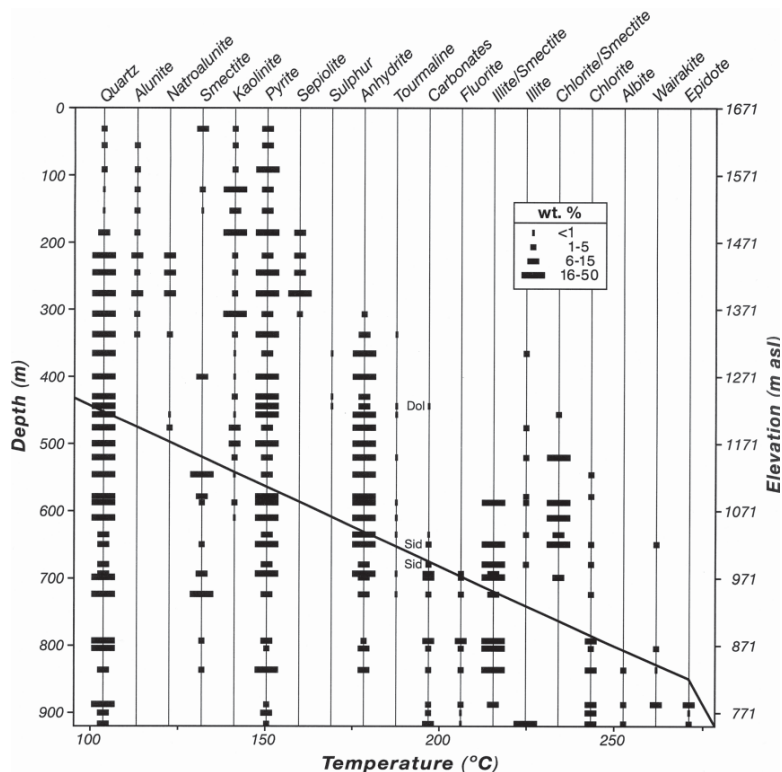


FIG. 4. Mineral distributions in the upper 900 m of core hole T-2. The solid line shows the downhole measured temperatures. The well recorded a maximum temperature of 321°C at its base (1383 m, 288 m asl). The carbonate minerals include calcite (unlabeled), dolomite (dol) and siderite (sid).

of 475 m. The alunite-supergroup minerals encapsulate pyrite and are in turn cut by later veins of pyrite.

The alunite and natroalunite occur as coarse blades up to 0.15 mm long and 0.02 mm wide that replace phenocrysts and fill veins. Their coarse grain-size is typical of hypogene magmatic-hydrothermal environments (Thompson & Petersen 1991, Thompson 1991). Both alunite and natroalunite can display significant variability in their chemical compositions as a result of substitutions involving Na, K, $(\text{H}_3\text{O})^+$, P, S and NH_4 (e.g., Jambor 1999). Electron-microprobe analyses indicate the presence of up to 0.77 wt% N and 1.3 wt% P in samples from a depth of 220 m.

Anhydrite is the common stable sulfate-bearing mineral below ~350 m. It remains abundant to 750 m and then is present only sporadically in the deep parts of the well. Pyrite is the only sulfide mineral found in these rocks. It both predates and postdates anhydrite (Figs. 5A, B), although the bulk of the coarse-grained pyrite was deposited after anhydrite. Electron-microprobe

analyses indicate that the pyrite contains no detectable Au, Ag, As or Cu (Lutz & Moore 2002).

Between depths of 340 and 725 m, fine-grained needles and pale blue-green radiating aggregates of tourmaline are encapsulated in the anhydrite and in the occasional contemporaneous quartz (Fig. 5B). The average of seven electron-microprobe analyses of tourmaline from a depth of 634 m is presented in Table 1. The structural formula was calculated by normalizing the sum of the $T + Z + Y$ cations to 15 atoms per formula unit (Henry & Dutrow 1996). Because this approach does not make the assumption that all of the anion sites are filled with OH, it provides a means of estimating the total OH content. The calculations indicate that, on average, there is an excess charge of 0.62, which is a minimum estimate of the deprotonation of the OH. Thus, more than half of the W site is occupied by O. In addition, there is a significant alkali-deficiency in the X site. Compositionally, the tourmaline can be classified as an "oxy-dravite" with an appreciable magnesiofoitite com-

ponent (Hawthorne & Henry 1999, D. Henry, pers. commun., 2003).

Tourmaline is not commonly observed at shallow depths in epithermal and geothermal systems. Its occurrence in core hole T-2 near Telaga Bodas suggests that its formation is due to reactions between ascending magmatic H_3BO_3 and partially neutralized, descending acid-sulfate waters that have become enriched in cations through rock dissolution.

Wairakite, a common late-stage mineral throughout the field, occurs in the lower part of core hole T-2. It characteristically postdates anhydrite but predates calcite. Rarely, wairakite is intergrown with stage-2 quartz. Wairakite is found in many geothermal systems in which temperatures range from $\sim 210^\circ$ to 300°C . The precipitation of wairakite over epidote is favored by cooling or decreasing pH (Browne & Ellis 1970), and over prehnite, by decreasing pH (C. Bruton, pers. commun., 1996). The relationships at Karaha – Telaga Bodas suggest that wairakite, rather than epidote or prehnite, was deposited when residual reservoir waters mixed with the descending steam condensates following decompression of the fluids (Moore *et al.* 2000b).

At shallow depths in core hole T-2, the final stages of the paragenesis are represented by dolomite (Fig. 5C) and later, native sulfur (Fig. 5D). The sulfur is found at depths of 390 to 440 m. Siderite is the late carbonate at intermediate depths (680 m). In the deep parts of core hole T-2, calcite (Fig. 5E) followed by fluorite (Fig. 5F) represent the last stages in the paragenesis.

The rock surfaces in core holes T-2 and T-8 were subsequently coated with a variety of chemical precipitates. SEM-EDS analyses document precipitates of NaCl, KCl, $FeCl_x$ and Ti-Si-Fe (Fig. 6), and X-ray-diffraction analyses indicate the presence of halite. These precipitates are interpreted as representing the complete drying out of the descending condensates and remaining pore-fluids present within the low-pressure, but high-temperature vapor-dominated zone.

Fluid-inclusion systematics

The distribution of fluid-inclusion homogenization temperatures of stage-3 minerals with respect to elevation and the downhole-measured temperatures is shown in Figure 7. Fluid inclusions trapped in veins from core hole T-2 record temperatures that are similar to the measured conditions. In contrast, inclusions in core hole T-8 record a wider range of temperatures, documenting cooling to the present downhole values.

Figures 7 and 8 show a progressive change in the chemistry of the waters with depth, the measured downhole temperatures, and the homogenization temperatures of the inclusions. Inclusions in samples from elevations above 950 m asl have freezing-point depressions that decrease from 2.8° to 1.5°C as homogenization temperatures increase from $\sim 160^\circ$ to 205°C . The freezing-point depressions then remain nearly constant

although the homogenization temperatures increase to 235°C (Fig. 8).

Inclusions in samples from below 850 m asl yielded homogenization temperatures greater than 235°C . In contrast to the shallower inclusions, the freezing-point depressions increase with depth and increasing temperature (Fig. 8). Inclusions trapped in anhydrite from 586 m asl in core hole T-8 contain halite-saturated fluid with a salinity of 31 wt.% NaCl equivalent. The occurrence of chemical precipitates on anhydrite containing hypersaline fluids indicates that boiling toward dryness caused the salinities to increase below elevations of 850 m asl, where temperatures exceed $\sim 250^\circ\text{C}$. Boiling, or combinations of boiling and mixing, however, will not explain the progressive decrease in the freezing-point depression of the fluids at shallower depths. Instead, the pressure – temperature – composition relationships suggest that this progressive change must be the result of mineral precipitation. In the following section, the effects of water–rock interactions on the composition of the fluids are described.

WATER–ROCK INTERACTIONS

Reaction-path simulations of the condensation of volcanic gas and subsequent water–rock interactions have been treated in detail by Christenson & Wood (1993) and Symonds (1998). Condensates associated with volcanic fumaroles are typically hyper-acidic (pH <1), consisting of dilute mixtures of H_2SO_4 and HCl. At temperatures $<250^\circ\text{C}$, these fluids generally precipitate elemental sulfur (S_e). The condensates aggressively attack unaltered rocks in the reservoir, and the ensuing hydrolysis reactions consume hydrogen ions, leading both to the re-dissolution of the elemental sulfur according to the reaction:



and an overall reduction in the oxidation state of the fluid through interaction with reduced iron in the rocks by the reaction:



which is the so-called rock redox buffer of Giggenbach (1987).

Water–rock interactions in the Karaha – Telaga Bodas system were simulated by numerically reacting lake water from Telaga Bodas (Table 2; unpubl. data) with rock of andesitic composition (Christenson & Wood 1993). The selection of Telaga Bodas water as representative of the acid-sulfate condensate component is based on the observation that assemblages of advanced argillic alteration are only observed in core hole T-2, which lies closest to the lake. Despite the apparently limited distribution of advanced argillic alteration at Karaha – Telaga Bodas, this style of alteration and

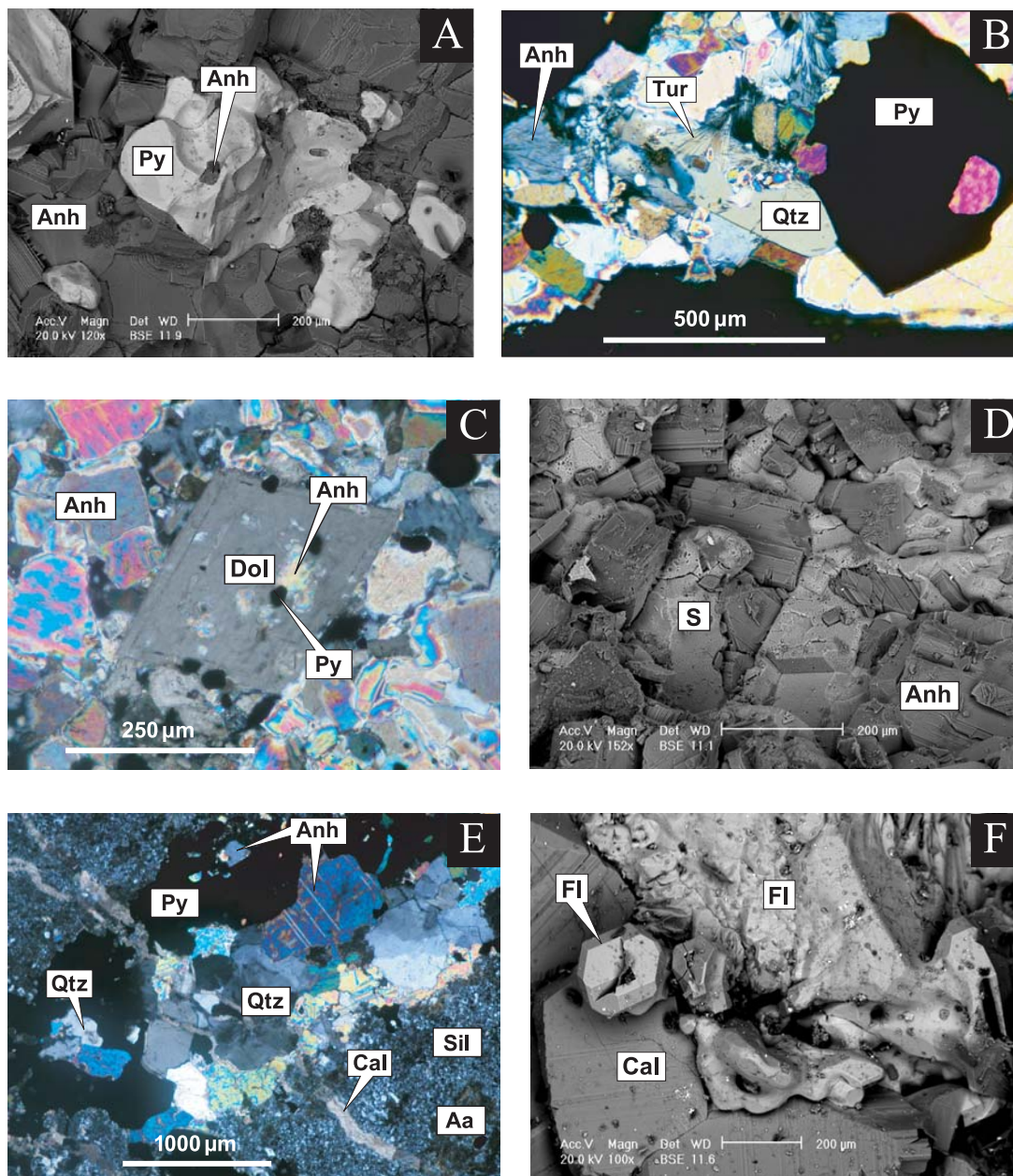


FIG. 5. Characteristic mineral textures. All images are from core hole T-2. A) SEM – back-scattered electron image of pyrite (py) replacing anhydrite (anh). Remnants of anhydrite are encapsulated in the pyrite. From a depth of 679 m; scale bar: 200 μm . B) Fine-grained needles of tourmaline (tur) are encapsulated in anhydrite (anh) and quartz (qtz). The pyrite (py) encapsulates anhydrite and is coated by later anhydrite. From a depth of 634 m. Crossed nicols. C) Dolomite (dol) after anhydrite (anh) and pyrite (py). From a depth of 442 m. Crossed nicols. D) SEM – back-scattered electron image of native sulfur (S) after anhydrite (anh). From a depth of 434 m; scale bar: 200 μm . E) Altered and veined pyroclastic deposit displaying the progressive effects of the early liquid-dominated system [pervasive argillic alteration (aa) and later silicification (sil)], decompression [quartz (qtz)], and descending steam condensate [anhydrite (anh), followed by pyrite (py) and then calcite (cal)]. From a depth of 694 m. Crossed nicols. F) SEM – back-scattered electron image of fluorite (fl) after calcite (cal). From a depth of 793 m; scale bar: 200 μm .

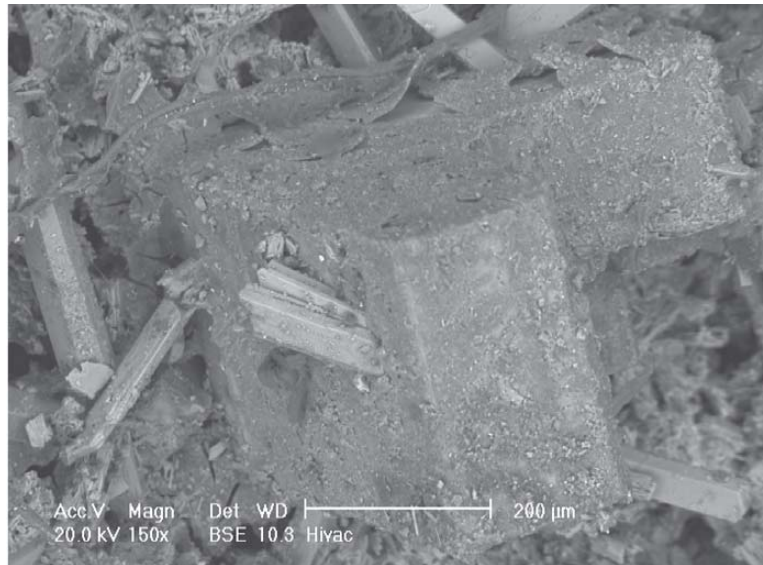


FIG. 6. SEM – back-scattered electron image of anhydrite coated with a Ti-rich precipitate. The anhydrite encapsulates crystals of epidote. The sample is from a depth of 1045 m (586 m asl) in core hole T-8. Anhydrite from this depth contains inclusions of halite-saturated fluid. Scale bar: 200 μm.

TABLE 1. AVERAGE COMPOSITION OF TOURMALINE FROM A DEPTH OF 634 M IN CORE HOLE T-2, KARAHIA – TELAGA BODAS GEOTHERMAL SYSTEM, INDONESIA

| | | | | | |
|------------------------------------|-------|-------------|------------------|-------|--------------|
| B ₂ O ₃ wt.% | 10.77 | <i>0.13</i> | B <i>apfu</i> | 3 | |
| SiO ₂ | 36.85 | <i>0.85</i> | Si | 5.952 | <i>0.085</i> |
| Al ₂ O ₃ | 36.36 | <i>0.65</i> | ³ Al | 0.048 | |
| TiO ₂ | 0.15 | <i>0.08</i> | ⁴ Al | 6 | |
| FeO | 1.02 | <i>0.63</i> | ³ Al | 0.874 | <i>0.069</i> |
| MnO | 0.06 | <i>0.01</i> | Ti | 0.018 | <i>0.010</i> |
| MgO | 8.15 | <i>0.40</i> | Fe ²⁺ | 0.138 | <i>0.086</i> |
| CaO | 0.81 | <i>0.22</i> | Mn | 0.008 | <i>0.002</i> |
| Na ₂ O | 1.55 | <i>0.14</i> | Mg | 1.962 | <i>0.097</i> |
| K ₂ O | 0.03 | <i>0.02</i> | Ca | 0.141 | <i>0.038</i> |
| F | 0.22 | <i>0.05</i> | Na | 0.485 | <i>0.049</i> |
| Cl | 0.06 | <i>0.04</i> | K | 0.005 | <i>0.003</i> |
| Total | 96.01 | <i>1.15</i> | [□] | 0.369 | <i>0.034</i> |
| O – F, Cl | 0.11 | | F | 0.112 | <i>0.026</i> |
| Total | 95.91 | | Cl | 0.016 | <i>0.011</i> |
| | | | OH | 3.257 | <i>0.135</i> |
| | | | O | 0.615 | <i>0.149</i> |

Note: B₂O₃, OH and O determined by stoichiometry (e.g., Hlawthorne 1996, Henry & Dutrow 1999). Fe is assumed to be all Fe²⁺. Standard deviations are given in italics. The standard deviation given for ³Al is for total Al. The composition is the average of seven determinations (electron-microprobe analyses). The atomic proportions, quoted in atoms per formula unit (*apfu*), are based on the sum of Y + Z + T cations normalized to 15.

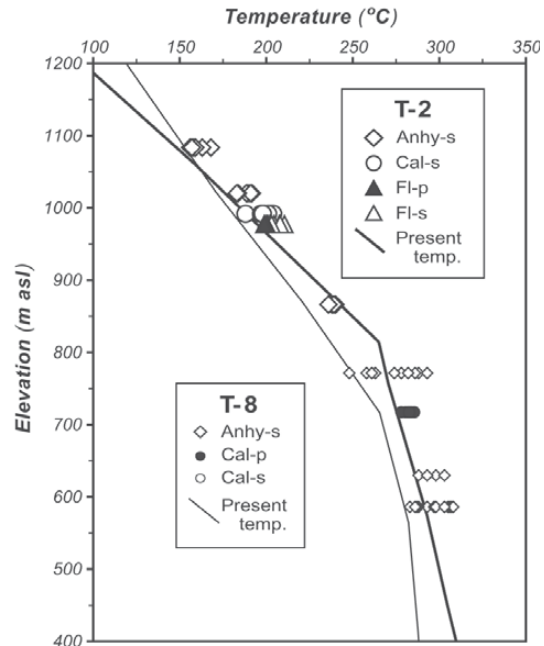


FIG. 7. Homogenization temperatures of fluid inclusions in stage-3 minerals from core holes T-2 and T-8. For reference, the measured downhole temperatures are shown. The data are plotted with respect to elevation (m asl). Abbreviations: anhy: anhydrite, cal: calcite, fl: fluorite, p: primary, s: secondary. The top of core hole T-2 is located at an elevation of 1671 m asl; core hole T-8 is located at 1631 m asl.

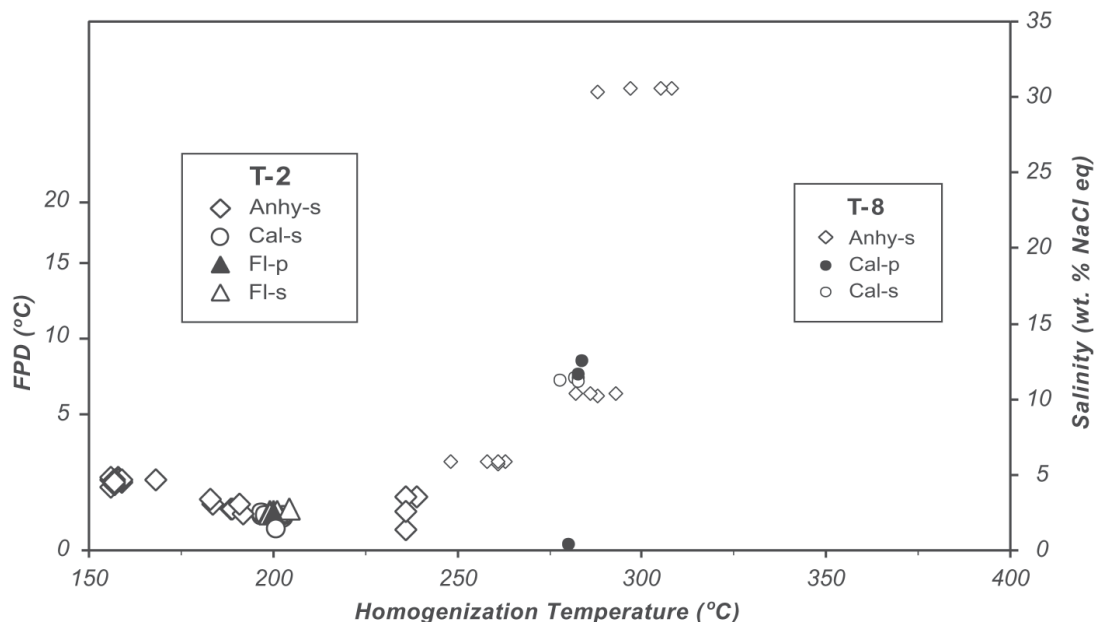


FIG. 8. Homogenization temperatures and freezing-point depressions (FPD) of individual fluid-inclusions from the stage-3 minerals shown in Figure 7. Salinities, expressed as wt.% NaCl equivalent, are shown on the right. Abbreviations as in Figure 7.

TABLE 2. COMPOSITION OF TELAGA BODAS WATER, KARAHA - TELAGA BODAS GEOTHERMAL SYSTEM, INDONESIA

| Ca | Mg | Na | K | SO ₄ | Cl | B | SiO ₂ | As | Fe | Sr | NH ₄ |
|-----|-----|-----|------|-----------------|------|-----|------------------|-------|------|-----|-----------------|
| 394 | 206 | 122 | 30.1 | 30500 | 8850 | 1.3 | 348 | 0.098 | 2320 | 1.4 | 13.9 |

Date of sampling: October 22, 1997. The pH, 0.4, was calculated for 20°C from ion-balance criteria. The chemical data are reported in mg/L, and were provided by the Karaha Bodas Co. LLC.

the associated veins of calcite and anhydrite are a common feature of many geothermal and volcanic systems. Thus the results of the numerical model developed here are considered to be broadly representative of the processes that occur as acidic waters descend.

The calculations were performed using the reaction-path simulator REACT (Bethke 1992). Initially, the lake water is considered to be in equilibrium with elemental sulfur, which is present on the lake floor. The calculations show that pyrite is also saturated in the lake at 20°C. CO₂ concentrations in the condensate have been set at 0.16 molal, which is typical of arc-type volcanic systems (Christenson *et al.* 2002).

Fluid temperatures were incrementally increased from 20° to 250°C to model descent of the condensate and simulate conductive heating of the fluids. In addi-

tion, the model was run on a "flow-through" basis, where 1 kg of condensate equilibrates with a total of 200 g of andesite in 100 steps (*i.e.*, 2 g per step), and the reacting fluids are isolated from solid reaction-products after each progress step. This best simulates the early development of the magmatic-hydrothermal vapor system.

DISCUSSION

The simulated assemblages of alteration minerals and solution pH are portrayed as a function of temperature in Figure 9. The simulations predict that quartz, anhydrite, alunite and kaolinite will predominate at temperatures <100°C and a pH <2. Anhydrite, clinocllore, montmorillonite, pyrite and hematite are the major phases at temperatures of 100° to 225°C and over a pH range of 2–5. At higher temperatures (225° to 250°C) and a neutral pH of 5 to 6, calcite and magnetite become stable. The predicted assemblages and their distributions agree closely with those observed in the altered rocks (*cf.* Fig. 4).

The relationship between time and space with respect to hydrothermal alteration in volcanic-hydrothermal systems is commonly difficult to resolve. Indeed, recent transport modeling by White & Christenson (2003) shows that a wide range of alteration minerals may form

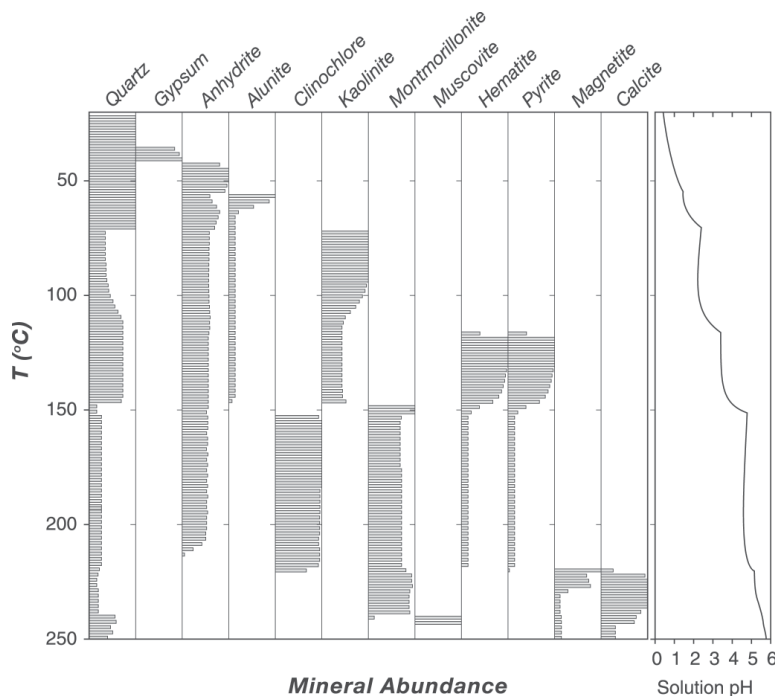


FIG. 9. Simulated assemblages of minerals resulting from the reaction of 1 kg of modified Telaga Bodas water with 200 g of andesite. The length of the bar gives the relative abundance of each mineral. Calculated pH values are shown on the right.

in environments where both fracture and intergranular permeability affect the processes controlling fluid migration (*e.g.*, convection *versus* diffusion). We consider the results presented here to be broadly representative of a fluid-dominated environment, which occurs in fracture channels, but it should be stressed that near-neutral pH conditions and different alteration-induced assemblages may coexist within the lower-permeability reservoir rocks nearby.

Effects of water–rock interactions on fluid-inclusion salinities

The correspondence between the observed and simulated assemblages of minerals suggests that the models can be used to interpret the observed progression in the freezing-point depressions (FPD) of the inclusion fluids. Although freezing-point depressions are normally represented as NaCl equivalents, the high concentrations of SO_4 relative to Cl in steam condensates suggest that the fluid-inclusion compositions may be better represented in terms of H_2SO_4 equivalents.

The freezing-point depression is a colligative property, which under ideal conditions is dependent only on

the concentration and not the nature of the solute (Atkins 1978). For aqueous solutions, the ideal relationship is:

$$\text{FPD} = 1.86 * \sum_{n=1}^i m_i \quad (3)$$

where FPD is the freezing-point depression, and m_i is molality of the i^{th} species.

In Figure 10, we demonstrate that the effect of NaCl solutions on the freezing-point depression remains close to ideal for concentrations up to 5 molal. The effects of H_2SO_4 , on the other hand, depart strongly from ideal behavior at concentrations above ~ 1.5 molal, suggesting that this non-ideality should be accounted for in the highly concentrated H_2SO_4 solutions that could be encountered in magmatic hydrothermal systems.

The relationship between the freezing-point depression and molality of H_2SO_4 solutions is given by the relationships:

$$\text{FPD} = 3.4703 m + 0.5600 m^2 - 0.0217 m^3 + 0.0383 m^4 - 1.0776E-3 m^5 \quad (4)$$

$$m = 0.2849 \text{ FPD} - 0.0104 \text{ FPD}^2 + 3.0503E-4 \text{ FPD}^3 - 5.9083E-6 \text{ FPD}^4 + 6.4972E-8 \text{ FPD}^5 - 3.0148E-10 \text{ FPD}^6 \quad (5)$$

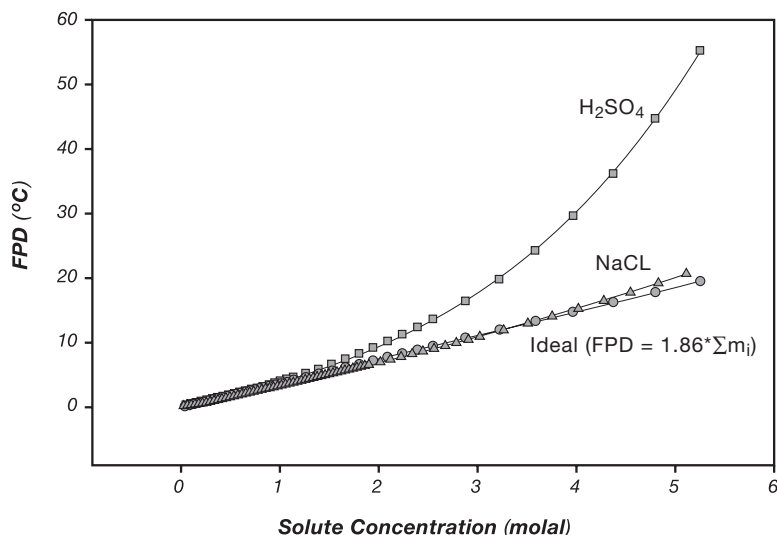


FIG. 10. Freezing-point depression (FPD) effects due to non-ideal behavior in NaCl and H₂SO₄ solutions. Experimental data for NaCl and H₂SO₄ are from Weast & Selby (1976).

For concentrations above 1.5 molal, calculation of salinities on a NaCl-equivalent basis will yield higher values than salinities based on H₂SO₄ equivalents. The measured concentrations of SO₄ in the Karaha – Telaga Bodas fluid, however, suggests that the non-ideality contribution to the freezing-point depression in the shallower, lower-temperature environments is probably not significant.

The results of the reaction-path modeling indicate that the inverse correlation between fluid-inclusion salinity and homogenization temperature can be explained, at least in part, by uptake of SO₄ and acid neutralization of the descending acid-sulfate condensate. As shown in Figure 11, the simulated freezing-point depressions of the fluid decrease from ~2.1 to 0.9°C (a decrease from ~3.6 to 1.6 wt.% NaCl equivalent) as SO₄ concentrations decrease from >30,000 mg/L (lake-water composition) to <1 mg/L in the acid-neutralized fluid at 250°C. The relatively high residual salinity of the acid-neutralized fluid can, in this case, be attributed largely to the combined effects of Cl (which behaves conservatively) and unreacted CO₂.

CONCLUSIONS

Downward percolating acid-sulfate waters are a common feature of many geothermal systems. Condensates associated with boiling hydrothermal fluids are characteristically SO₄-rich but Cl-poor. These fluids aggressively react with the host rocks, leaving a distinct

mineralogical signature characterized by alunite-supergroup minerals and a variety of clays that are stable in low-pH environments. At Karaha – Telaga Bodas, descending steam condensates have produced advanced argillic alteration that is superseded at depth by veins dominated by anhydrite, pyrite, calcite and, locally, fluorite. Fluid inclusions trapped in anhydrite, calcite and fluorite provide a unique record of the chemical and thermal evolution of the fluids. The data indicate that the freezing-point depressions and, hence, the apparent salinities of the fluids, first decrease as the homogenization temperatures increase from ~160° to 205°C, then remain approximately constant to 235°C. At higher temperatures and greater depths, the fluids boil off, eventually becoming hypersaline as temperatures reach 300°C.

The evolution of descending steam condensate between temperatures of 20° and 250°C was numerically simulated using the composition of acidic water from Telaga Bodas and rock of andesitic composition. These simulations have yielded mineral assemblages and fluid-freezing temperatures that are in close agreement with the observed relationships.

Freezing-point depressions of the simulated descending steam condensate initially decrease as the fluid is heated from 20° to 220°C and hydrothermal minerals remove SO₄. At higher temperatures, between ~220° and 250°C, the freezing-point depressions of the modeled fluid remain nearly constant, as do the inclusion fluids. The modeling results indicate that Cl and residual CO₂ control the freezing-point depression of the fluids at these temperatures.

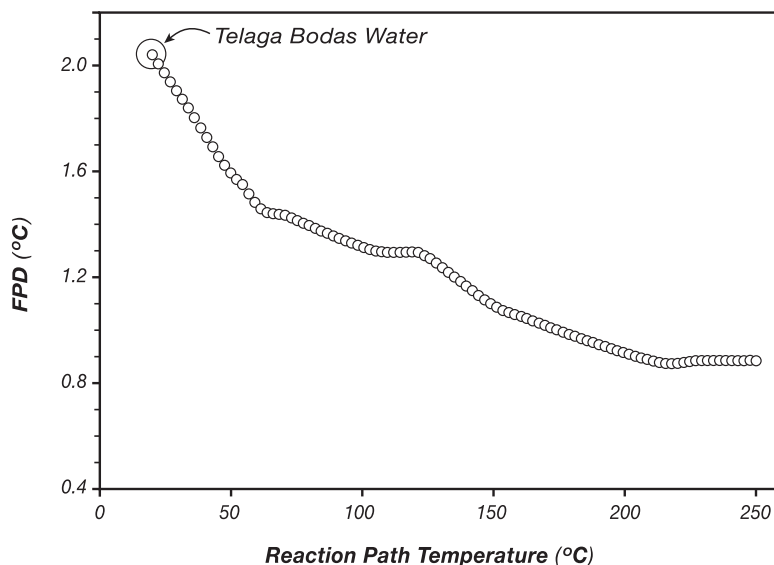


FIG. 11. Simulated effect of water–rock interactions on the freezing-point depression (FPD) of acid condensate.

Compilations of freezing-point depressions for NaCl and H₂SO₄ solutions indicate that there are substantial differences in the behavior of these fluids at moderate to high concentrations of solute. At concentrations >1.5 molal, freezing-point depressions expressed as NaCl equivalents will overestimate the salinity of a Cl-poor steam condensate. These differences may be important in interpreting fluid compositions trapped in high-sulfidation ore deposits and regions of advanced argillic alteration associated with degassing intrusions. However, at lower concentrations, between 0 and 1.5 molal, the differences in the calculated salinities are insignificant.

ACKNOWLEDGEMENTS

We are grateful to the management and staff of the Karaha Bodas Co. LLC for generously providing the samples and data used in this investigation. D. Henry and F.C. Hawthorne provided invaluable assistance in interpreting the tourmaline compositions. A computer program written by E. Peterson was used to calculate the structural formula of the tourmaline. J. Renner graciously provided access to the scanning electron microscope at the Idaho National Engineering and Environmental Laboratory. M. Hankin deserves credit for the remarkable images. R. Lambert assisted with the electron-microprobe analyses, and L. Spann performed the X-ray-diffraction analyses. D. Jensen patiently drafted the figures. Critical reviews by D. Love, D. Norman and R.F. Martin greatly improved the manuscript. We thank

them all. Funding for JNM and SJL was provided under DOE contract DE-PS07-98ID13589.

REFERENCES

- ALLIS, R., MOORE, J., MCCULLOCH, J., PETTY, S. & DEROCHE, T. (2000): Karaha – Telaga Bodas, Indonesia: a partially vapor-dominated geothermal system. *Geotherm. Res. Counc. Trans.* **24**, 217-222.
- AREHART, G.B., KESLER, S.E., O'NEIL, J.R. & FOLAND, K.A. (1992): Evidence for the supergene origin of alunite in sediment-hosted micron gold deposits, Nevada. *Econ. Geol.*, **87**, 263-270.
- ATKINS, P.W. (1978): *Physical Chemistry*. Oxford University Press, Oxford, U.K.
- BETHKE, C. (1992): *The Geochemists Workbench: a User's Guide to Rxn, Act2, Tact, React and Gtplot*. Univ. of Illinois, Chicago, Illinois.
- BODNAR, R.J. (1993): Revised equation and table for determining the freezing-point depression of H₂O–NaCl solutions. *Geochim. Cosmochim. Acta* **57**, 683-684.
- BRONTO, S. (1989): *Volcanic Geology of Galunggung, West Java, Indonesia*. Ph.D. thesis, Univ. of Canterbury, Canterbury, New Zealand.
- BROWNE, P.R.L. & ELLIS, A.J. (1970): The Ohaki–Broadlands hydrothermal area, New Zealand: mineralogy and related geochemistry. *Am. J. Sci.* **269**, 97-131.

- CHRISTENSON, B.W. (2000): Geochemistry of fluids associated with the 1995/96 eruption of Mt Ruapehu, New Zealand: signatures and processes in the magmatic-hydrothermal system. *J. Volcan. Geotherm. Res.* **97**, 1-30.
- _____, MROCZEK, E.K., KENNEDY, B.M., VAN SOEST, M.C., STEWART, M.K. & LYON, G. (2002): Ohaki reservoir chemistry: characteristics of an arc-type hydrothermal system in the Taupo Volcanic Zone, New Zealand. *J. Volcan. Geotherm. Res.* **115**, 53-82.
- _____ & WOOD, C.P. (1993): Evolution of a vent-hosted hydrothermal system under Ruapehu Crater Lake, New Zealand. *Bull. Volcan.* **55**, 547-565.
- EBERT, S.W. & RYE, R.O. (1997): Secondary precious metal enrichment by steam-heated fluids in the Crofoot-Lewis hot spring gold-silver deposit and relation to paleoclimate. *Econ. Geol.* **92**, 578-600.
- ELLIS, A.J. & MAHON, W.A.J. (1977): *Chemistry and Geothermal Systems*. Academic Press, New York, N.Y.
- ESCHER, B.G. (1925): L'éboulement préhistorique de Tasikmalaya et le volcan Galoenggoeng Java. *Leid. Geol. Meded.* **1**, 8-21.
- FOURNIER, R.O. (1973): Silica in thermal waters: laboratory and field investigations. In Proc. Int. Symp. on Hydrogeochemistry and Biogeochemistry. 1. Hydrogeochemistry. J.W. Carl, Washington, D.C. (132-139).
- _____ (1985): The behavior of silica in hydrothermal solutions. In *Geology and Geochemistry of Epithermal Systems* (B.R. Berger & P.M. Bethke, eds.). *Rev. Econ. Geol.* **2**, 45-62.
- GIGGENBACH, W.F. (1987): Redox processes governing the chemistry of fumarolic gas discharges from White Island, New Zealand. *Appl. Geochem.* **2**, 143-161.
- HAWTHORNE, F.C. (1996): Structural mechanisms for light-element variations in tourmaline. *Can. Mineral.* **34**, 123-132.
- _____ & HENRY, D.J. (1999): Classification of the minerals of the tourmaline group. *Eur. J. Mineral.* **11**, 201-216.
- HAYBA, D.O., BETHKE, P.M., HEALD, P. & FOLEY, N.K. (1985): Geologic, mineralogic, and geochemical characteristics of volcanic-hosted epithermal precious-metal deposits. In *Geology and Geochemistry of Epithermal Systems* (B.R. Berger & P.M. Bethke, eds.). *Rev. Econ. Geol.* **2**, 129-167.
- HEDENQUIST, J.W. (1990): The thermal and geochemical structure of the Broadlands-Ohaaki geothermal system, New Zealand. *Geothermics* **19**, 151-185.
- _____ (1995): The ascent of magmatic fluid: discharge versus mineralization. In *Magmas, Fluids, and Ore Deposits* (J.F.H. Thompson, ed.). *Mineral. Assoc. Can., Short Course Ser.* **23**, 263-289.
- _____, MATSUHISA, Y., IZAWA, E., WHITE, N.C., GIGGENBACH, W.F. & AOKI, M. (1994): Geology, geochemistry, and origin of high sulfidation Cu-Au mineralization in the Nansatsu District, Japan. *Econ. Geol.* **89**, 1-30.
- HEMLEY, J.J., HOSTETLER, P.B., GUDE, A.J. & MOUNTJOY, W.T. (1969): Some stability relations of alunite. *Econ. Geol.* **64**, 599-612.
- _____, MONTOYA, J.W., MARINENKO, J.W. & LUCE, R.W. (1980): Equilibria in the system Al_2O_3 - SiO_2 - H_2O and some general implications for alteration-mineralization processes. *Econ. Geol.* **75**, 210-228.
- HENLEY, R.W. & ELLIS, A.J. (1983): Geothermal systems ancient and modern: a geochemical review. *Earth-Sci. Rev.* **19**, 1-50.
- HENRY, D.J. & DUTROW, B.L. (1996): Metamorphic tourmaline. In *Boron: Mineralogy, Petrology and Geochemistry* (E.S. Grew & L.M. Anovitz, eds.). *Rev. Mineral.* **33**, 503-557.
- JAMBOR, J.J. (1999): Nomenclature of the alunite supergroup. *Can. Mineral.* **37**, 1323-1341.
- KUSAKABE, M., KOMODA, Y., TAKANO, B. & ABIKO, T. (2000): Sulfur isotopic effects in the disproportionation reaction of sulfur dioxide in hydrothermal fluids: implications for the $\delta^{34}S$ variations of dissolved bisulfate and elemental sulfur from active crater lakes. *J. Volcan. Geotherm. Res.* **97**, 287-307.
- LUTZ, S.J. & MOORE, J.N. (2002): Alteration mineralogy and trace element geochemistry of the Karaha - Telaga Bodas geothermal system, Indonesia - assessing fluid sources and behaviors. *Soc. Econ. Geol., Global Explor. 2002: Integrated Methods for Discovery*, 120 (abstr.).
- MAHON, W.A.J., KLYEN, L.E. & RHODE, M. (1980): Natural sodium-bicarbonate-sulphate hot waters in geothermal systems. *Chinetsu (J. Japanese Energy Assoc.)* **17**, 11-24.
- MOORE, J.N., ALLIS, R., RENNER, J.L., MILDENHALL, D. & McCULLOCH, J. (2002a): Petrologic evidence for boiling to dryness in the Karaha - Telaga Bodas geothermal system, Indonesia. *Proc. 27th Workshop Geotherm. Reservoir Eng., Stanford Univ.*, 223-232.
- _____, LUTZ, S.J., RENNER, J.L., McCULLOCH, J. & PETTY, S. (2000a): Evolution of a volcanic-hosted vapor-dominated system: petrologic and geochemical data from corehole T-8, Karaha - Telaga Bodas, Indonesia. *Geotherm. Res. Council Trans.* **24**, 259-263.
- _____, NORMAN, D.I. & ALLIS, R.G. (2002b): Geochemical evolution of the vapor-dominated regime at Karaha - Telaga Bodas, Indonesia: insights from fluid inclusion gas compositions. *Proc. 24th N. Z. Geotherm. Workshop, Auckland Univ.*, 243-248.
- _____, POWELL, T.S., HEIZLER, M.T. & NORMAN, D.I. (2000b): Mineralization and hydrothermal history of the Tiwi geothermal system, Philippines. *Econ. Geol.* **95**, 1001-1023.
- POUCHOU, J.L. & PICOIR, F. (1991): Quantitative analysis of homogeneous or stratified microvolumes applying the

- model "PAP". In *Electron Probe Quantification* (K.F.J. Heinrich & D.E. Newbury, eds.). Plenum Press, New York, N.Y. (31-75).
- POWELL, T., MOORE, J., DEROCHE, T. & MCCULLOCH, J. (2001): Reservoir geochemistry of the Karaha – Telaga Bodas prospect, Indonesia. *Geotherm. Res. Council Trans.* **25**, 363-367.
- REYES, A.G. (1990): Petrology of Philippine geothermal systems and the application of alteration mineralogy to their assessment. *J. Volcan. Geotherm. Res.* **43**, 279-309.
- _____ (1991): Mineralogy, distribution and origin of acid alteration in Philippine geothermal systems. In *High-Temperature Acid Fluids and Associated Alteration and Mineralization* (Y. Matsuhisa, A. Masahiro & J. Hedenquist, eds.). *Geol. Surv. Japan, Rep.* **277**, 59-65.
- SANDER, M.V. & BLACK, J.E. (1988): Crystallization and recrystallization of growth-zoned vein quartz crystals from epithermal systems – implications for fluid inclusion studies. *Econ. Geol.* **83**, 1052-1060.
- STERNER, S.M., HALL, D.L. & BODNAR, R.J. (1988): Synthetic fluid inclusions. V. Solubility relations in the system NaCl–KCl–H₂O under vapor-saturated conditions. *Geochim. Cosmochim. Acta* **52**, 989-1005.
- STOFFREGEN, R.E. (1987) Genesis of acid-sulfate alteration and Au–Cu–Ag mineralization at Summitville, Colorado. *Econ. Geol.* **82**, 1575-1591.
- SYMONDS, R.B. (1998): Modeling the interaction of magmatic gases with water at active volcanoes. *Proc. 9th Int. Symp. Water–Rock Interaction (Taupo)*, 495-498.
- THOMPSON, A.J.B. (1991) Characteristics of acid-sulfate alteration in the Marysvale–Pioche Mineral Belt: a guide to gold mineralization: *Utah Geol. Surv., Misc. Publ.* **91-2**.
- _____ & PETERSEN, E.U. (1991): Alunite compositions and textures: indicators of the environment of formation. *Geol. Soc. Am., Abstr. Program*, A229.
- TRIPP, A., MOORE, J., USHER, G. & MCCULLOCH, J. (2002): Gravity modeling of the Karaha – Telaga Bodas geothermal system, Indonesia. *Proc. 27th Workshop Geotherm. Reservoir Eng., Stanford Univ.*, 444-452.
- WEAST, R.C. & SELBY, S.M. (1976): *Handbook of Chemistry and Physics*. The Chemical Rubber Company, Cleveland, Ohio (D-176).
- WHITE, N.C. & HEDENQUIST, J.W. (1990): Epithermal environments and styles of mineralization: variations and their causes, and guidelines for exploration. *J. Geochem. Explor.* **36**, 445-474.
- WHITE, S.P. & CHRISTENSON, B.W. (2003): Modeling two-phase fracture flow above a diorite intrusion. *Proc. 24th N. Z. Geotherm. Workshop, Auckland Univ.*, 97-102.
- YANATIEVA, O.K. (1946): Polythermal solubilities in the systems CaCl₂–MgCl₂–H₂O and CaCl₂–NaCl–H₂O. *Zh. Priklad. Khim.* **19**, 709-722 (in Russ.).

Received November 8, 2002, revised manuscript accepted October 31, 2003.